

TECHNICAL NOTE

Enhancement of bearing capacity from consolidation: due to changing strength or failure mechanism?

S. A. STANIER* and D. J. WHITE†

Bearing capacity of shallow foundations is higher following preload (or self-weight)-induced consolidation because the soil strength changes, and perhaps because the failure mechanism changes. Previous studies have illustrated this effect by plotting or predicting changes in either bearing capacity factor or strength. In this study, the relative contribution of these two effects is explored. This is achieved by formalising a definition of bearing capacity factor, which is described in terms of the average strength mobilised in the deformation mechanism at failure. Using the alternative definition of bearing capacity factor, the gain in foundation capacity is shown to be almost entirely due to changes in soil strength, rather than bearing capacity factor, which remains largely unaffected by the strength gains. This observation should encourage future studies into consolidated bearing capacity to present gains in capacity in terms of changes in mobilised strength rather than changes in bearing capacity factors, and supports the use of prediction methods that focus on defining the change in soil strength.

KEYWORDS: bearing capacity; consolidation; footings/foundations; numerical modelling; shear strength

INTRODUCTION

When a foundation is placed on soft clay, the self-weight or sustained vertical load causes consolidation of the soil, resulting in an increase in the bearing capacity of the foundation over time. The prediction and utilisation of this gain in bearing capacity allow more efficient foundation design. Previous studies have observed this behaviour by way of model-scale experiments (Lehane & Gaudin, 2005; Bienen & Cassidy, 2013; Stanier *et al.*, 2014; Vulpe & White, 2014; Vulpe *et al.*, 2016a, 2016b), numerical simulations (Bransby, 2002; Zdravkovic *et al.*, 2003; Gourvenec *et al.*, 2014; Fu *et al.*, 2015; Feng & Gourvenec, 2016) and field tests (Lehane & Jardine, 2003; Gaone *et al.*, 2018).

For a simple plane-strain shallow foundation on normally consolidated fine-grained soil (Fig. 1) the ultimate bearing capacity, V_u , is linked to the in situ soil strength by way of a bearing capacity factor, N_{cv} , defined as

$$N_{cv} = \frac{V_u}{Bs_{um}} \approx f\left(\frac{kB}{s_{um}}\right) \quad (1)$$

where B is the footing width; s_{um} is the undrained strength at the mudline; and k is the gradient of strength with depth. The bearing capacity factor is often given as a function of the dimensionless parameter, kB/s_{um} , which describes the uniformity of the soil strength with depth. For horizontal and moment loading, similar capacity factors can

be defined as follows

$$N_{ch} = \frac{H_u}{Bs_{um}} \quad (2)$$

$$N_{cm} = \frac{M_u}{B^2 s_{um}} \quad (3)$$

If the foundation is subjected to a maintained preload, V_p (where $V_p < V_u$), excess pore pressure is initially created. This pore pressure dissipates, leading to consolidation and varying levels of strength gain in the surrounding soil. This change in strength distribution causes a gain in foundation bearing capacity, which can be linked to two potential effects: (a) the increase in the undrained strength, s_u , of the soil that fails when the bearing capacity is reached and (b) a change in the deformation mechanism at failure due to the change in distribution of soil strength beneath the foundation. In developing methods to predict the increase in foundation capacity due to preloading some researchers describe modifications to the bearing capacity factor and use the in situ strength profile (e.g. Bienen & Cassidy, 2013; Stanier *et al.*, 2014), whereas others have framed the behaviour as a change in the strength (e.g. Gourvenec *et al.*, 2014; Feng & Gourvenec, 2015). To develop simple prediction tools for changing bearing capacity, it is useful to understand the relative importance of these two effects so as to rationalise which is the most appropriate approach, and focus attention on the controlling aspect of the behaviour.

In this technical note, this uncertainty is tackled by separating the two effects using a specific definition of the bearing capacity factor that links it to the deformation mechanism. This allows the separate effects of the changing soil strength and the changing failure mechanism to be quantified explicitly.

DEFINITION OF BEARING CAPACITY FACTOR, N_c

A definition for the bearing capacity factor, N_c , is now introduced to distinguish the effects of soil strength and

Manuscript received 19 June 2017; revised manuscript accepted 20 February 2018. Published online ahead of print 16 April 2018. Discussion on this paper closes on 1 July 2019, for further details see p. ii.

* Centre for Offshore Foundation Systems, University of Western Australia, Crawley, WA, Australia (Orcid:0000-0001-5671-2902).

† Centre for Offshore Foundation Systems, University of Western Australia, Crawley, WA, Australia.

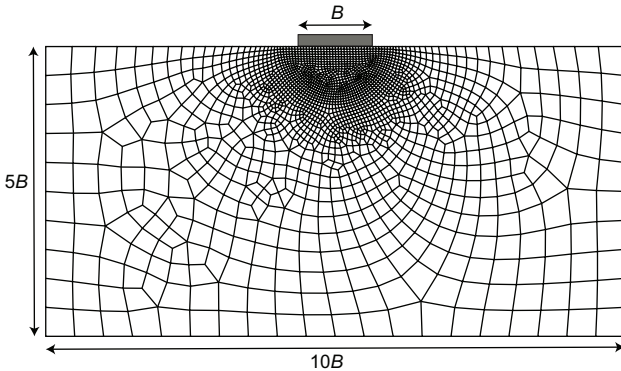


Fig. 1. Schematic diagram of plane-strain shallow foundation problem and finite-element analysis mesh

failure mechanism in numerical analyses. Instead of using the in situ mudline strength, s_{um} , in the normalisation of bearing capacity (equations (1)–(3)), the current authors use the average mobilised undrained strength at failure, $\bar{s}_{\text{u,mob}}$, defined as

$$\bar{s}_{\text{u,mob}} = \frac{\int_{\text{vol}} \Delta \gamma s_{\text{u}} \, d\text{vol}}{\int_{\text{vol}} \Delta \gamma \, d\text{vol}} \quad (4)$$

where $\Delta \gamma$ is the incremental shear strain, s_{u} is the undrained strength in each element of soil within the deformation mechanism and the integration is performed over the volume of the analysis domain. At failure under constant load, only plastic strain increments contribute to the integral, with elastic components being zero. Then, using this value the vertical bearing capacity factor, N_{cv} , is redefined as

$$N_{\text{cv}} = \frac{V_{\text{u}}}{B \bar{s}_{\text{u,mob}}} \quad (5)$$

For horizontal and moment loading it is possible to define similar capacity factors as follows

$$N_{\text{ch}} = \frac{H_{\text{u}}}{B \bar{s}_{\text{u,mob}}} \quad (6)$$

$$N_{\text{cm}} = \frac{M_{\text{u}}}{B^2 \bar{s}_{\text{u,mob}}} \quad (7)$$

where $\bar{s}_{\text{u,mob}}$ is evaluated for failure under the corresponding mode of loading.

If the change in strength dominates the variation in bearing capacity then the capacity factors calculated using the mobilised strength in this way will not change for different magnitudes or durations of preload. Alternatively, if any change in mechanism in itself has a significant effect on the capacity, the bearing capacity factors calculated using equations (5)–(7) will vary.

FINITE-ELEMENT ANALYSES

Parameters and analysis set-up

Small-strain finite-element analyses were performed using the modified Cam Clay (MCC) model in Abaqus, assuming a plane-strain footing with width, B , of 1 m, and rough interface conditions. Simple, first-order reduced integration coupled pore-fluid–effective stress elements (CPE4RP) were used in the analyses with a single, locally refined mesh for all cases (Fig. 1). The soil parameters are given in Table 1.

The soil was K_0 normally consolidated, with K_0 taken as

$$K_0 = 1 - \sin \phi_{\text{tc}} \approx 0.6 \quad (8)$$

Table 1. Modified Cam Clay parameters for UWA kaolin clay (after Stewart (1992))

| | |
|--|--------------------|
| Critical state friction angle for triaxial compression, ϕ_{tc} : degrees | 23.5 |
| Void ratio at $p' = 1$ kPa on CSL, e_{cs} | 2.14 |
| Slope of normal compression line in $e-\ln p'$ space, λ | 0.205 |
| Slope of recompression line in $e-\ln p'$ space, κ | 0.044 |
| Poisson ratio, ν | 0.3 |
| Effective unit weight, γ'_e : kN/m ³ | 7 |
| Permeability, k : m/s | 1×10^{-9} |

where ϕ_{tc} is the friction angle for triaxial compression. The initial size of the MCC yield envelope can be determined as

$$p'_c = \frac{q_0^2}{M^2 p'_0} + p'_0 \text{ with } M = \frac{6 \sin \phi_{\text{tc}}}{3 - \sin \phi_{\text{tc}}} \quad (9)$$

where p'_0 and q_0 are the initial mean effective stress and deviatoric stress, respectively. The initial voids ratio is calculated as

$$e_0 = e_{\text{N}} - \kappa \ln p'_0 - (\lambda - \kappa) \ln p'_c \quad (10)$$

where

$$e_{\text{N}} = e_{\text{cs}} + (\lambda - \kappa) \ln(2) \quad (11)$$

and λ and κ are the compression and swelling indices.

For plane-strain conditions the initial undrained strength is calculated following Wroth (1984)

$$s_{\text{u}} = \frac{2}{\sqrt{3}} \times \frac{\sin \phi_{\text{tc}}}{2a} \times \left(\frac{a^2 + 1}{2} \right)^{\Lambda} \sigma'_{v0} \quad (12)$$

where

$$a = \frac{3 - \sin \phi_{\text{tc}}}{2(3 - 2 \sin \phi_{\text{tc}})} \quad (13)$$

and

$$\Lambda = \frac{\lambda - \kappa}{\lambda} \quad (14)$$

Different levels of uniform stress were applied across the surface of the model to initialise the strength profile. Values were selected to generate dimensionless strength profiles, kB/s_{um} , of approximately 0.4, 2 and 4, which yield undrained strengths at the mudline, s_{um} , of 5.0, 1.0 and 0.5 kPa and a gradient of strength with depth, k , of 2.0 kPa.

Benchmarking for pure V, H and M loading

Pure vertical, horizontal and moment loading analyses were first run with no maintained preload period and loading applied sufficiently quickly that negligible drainage occurred. At the onset of failure for each soil profile, the vertical bearing capacity factors were no more than 8% higher than the equivalent Tresca analyses of Gourvenec & Randolph (2003) (linearly interpolating between the published bearing capacity factor values where necessary for kB/s_{um} not analysed in the original paper). For the horizontal and moment loading the discrepancy was slightly larger, but still less than 20% for all cases. These discrepancies are consistent with other coupled analyses of penetrometer penetration by Mahmoodzadeh *et al.* (2015), where ~9–12% more resistance was generated by the coupled MCC model compared to equivalent total stress approaches using the Tresca model. Even though loading is applied in the simulations sufficiently quickly that negligible drainage occurred, it is inevitable that

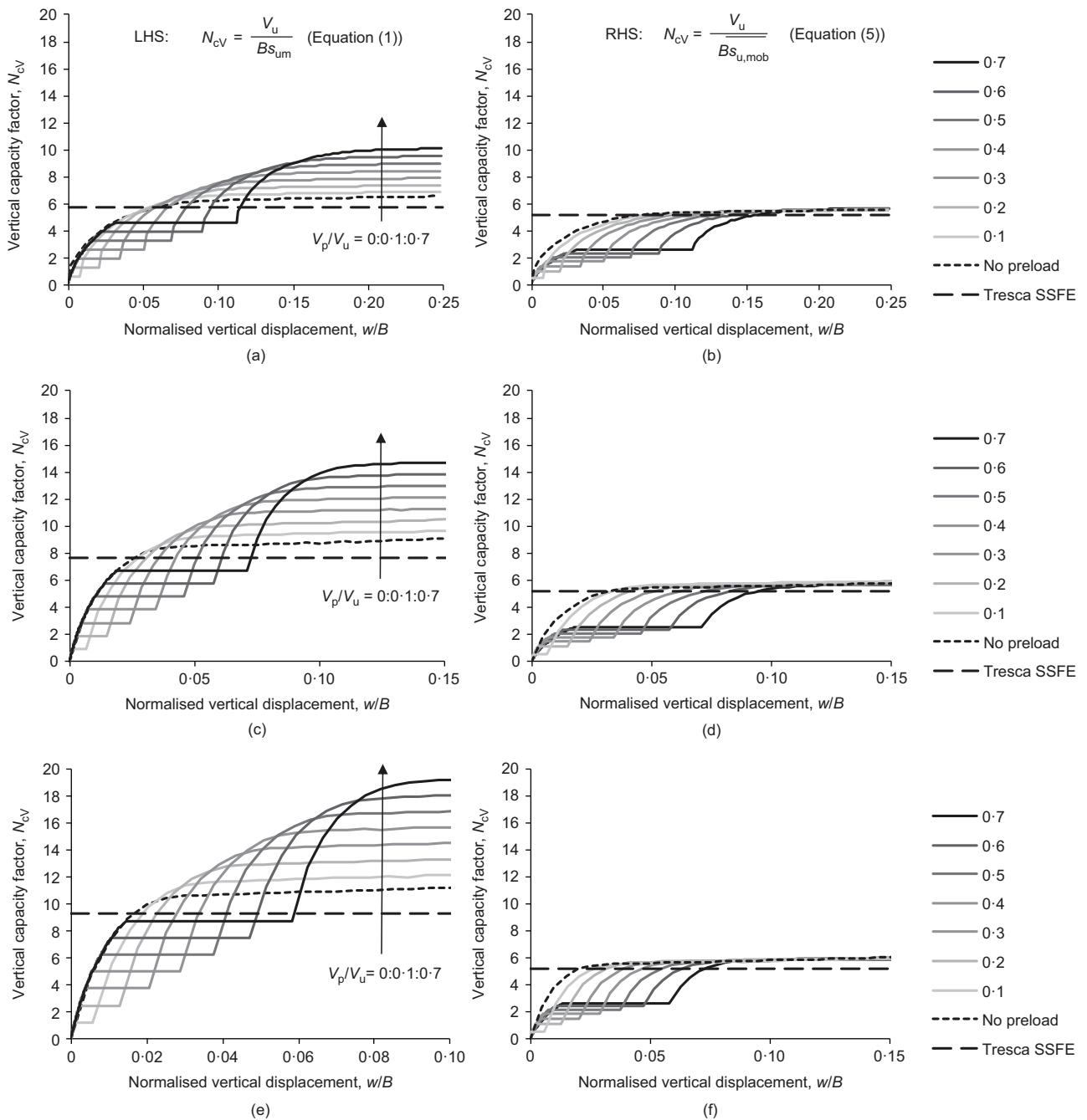


Fig. 2. Vertical bearing capacity (conventional normalisation, alternative normalisation): (a), (b) $kBs_{um} = 0.4$; (c), (d) $kBs_{um} = 2.0$; and (e), (f) $kBs_{um} = 4.0$

some local redistribution of excess pore pressures will lead to localised increases in strength during the loading process, particularly at the corners of the foundation where the drainage paths are shortest (Mahmoodzadeh *et al.*, 2015).

Further mesh refinement (e.g. finer meshes or fanned meshes with smaller elements at the corners of the foundation) could lead to a modest reduction in these discrepancies, which would be expected to yield the greatest improvement for the horizontal loading case (which shows the largest discrepancy compared to the Tresca small strain finite-element analyses of Gourvenec & Randolph (2003)) because the surface element largely controls the capacity at failure. However, the focus of this note is not the absolute bearing capacity but the changes in bearing capacity and failure mechanism, so, accepting these reservations, the mesh shown in Fig. 1 has been used for all subsequent analyses.

Parametric analysis for V , V_p-H and V_p-M cases

Additional analyses with preload ratios (V_p/V_u) over the range of 0.1–0.7 at intervals of 0.1 were then modelled, with time periods that allowed all excess pore pressures to dissipate. The consolidated undrained strength was calculated for each element in the finite-element analysis mesh as

$$s_{u,cons} = s_u \exp\left(\frac{e_0 - e_{cons}}{\lambda}\right) \quad (15)$$

where e_{cons} is the consolidated voids ratio, which can be calculated as

$$e_{cons} = [(1 + e_0)(1 + \varepsilon_v)] - 1 \quad (16)$$

where ε_v is the volumetric strain.

The foundation was then loaded to failure by applying further vertical, horizontal or rotational displacement at the

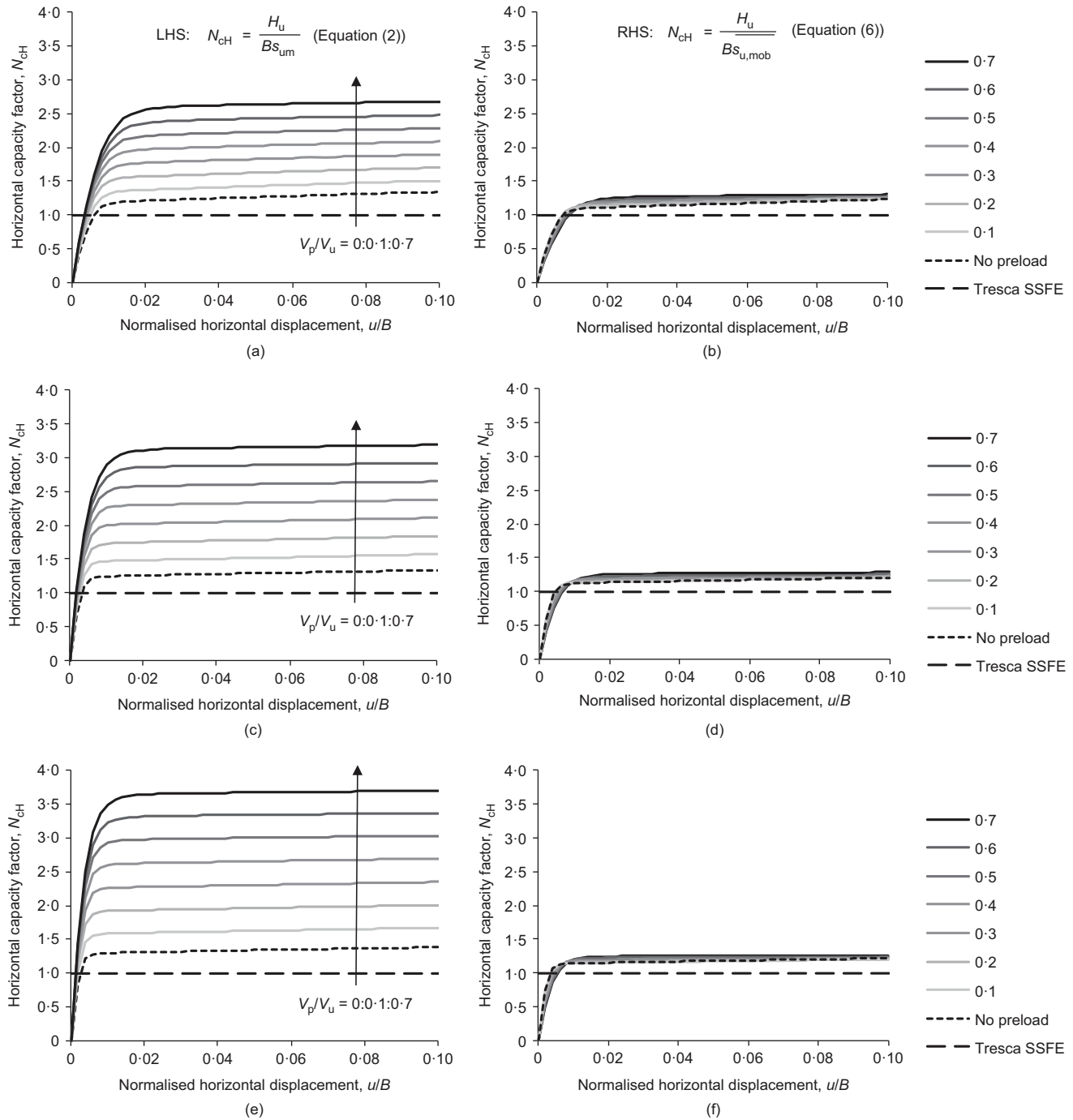


Fig. 3. Horizontal bearing capacity (conventional normalisation, alternative normalisation): (a), (b) $kB/s_{um} = 0.4$; (c), (d) $kB/s_{um} = 2.0$; and (e), (f) $kB/s_{um} = 4.0$

centre of the footing, with no constraint on all other degrees of freedom. For the horizontal and moment loading cases the vertical preload was maintained throughout, thereby simulating the self-weight of the foundation. The average mobilised undrained strength, $\overline{s}_{u,mob}$, was calculated for each analysis at the ultimate failure load for the final increment of displacement using equations (4), (12), (15) and (16), using the spatially varying consolidated undrained strength, $s_{u,cons}$, for the cases where a maintained preload was applied (i.e. $V_p/V_u > 0.0$). Alternative bearing capacity factors were then calculated using equations (5)–(7) and the values of $\overline{s}_{u,mob}$ were back-calculated for each analysis.

Figures 2–4 show the results of the analyses for all three strength profiles with the applied loads normalised by (a) the in situ undrained strength at the mudline, s_{um} , and (b) the

average mobilised undrained strength at failure, $\overline{s}_{u,mob}$, for vertical, horizontal and moment loading, respectively. For all loading modes the simulations are compared to bearing capacity factors derived from small-strain finite-element simulations for strip foundations on Tresca soil published by Gourvenec & Randolph (2003) (linearly interpolating between the values of kB/s_{um} published by Gourvenec & Randolph (2003)).

The bearing capacity factors for all failure modes and soil profiles collapse to approximately constant values close to the capacity factor for uniform conditions ($kB/s_{um} = 0.0$), irrespective of the preload ratio applied. Scrutinising the incremental shear strain fields ($\Delta\gamma$) at failure indicated that this convergence towards a constant bearing capacity factor – when the applied loads are normalised by $\overline{s}_{u,mob}$ – occurs

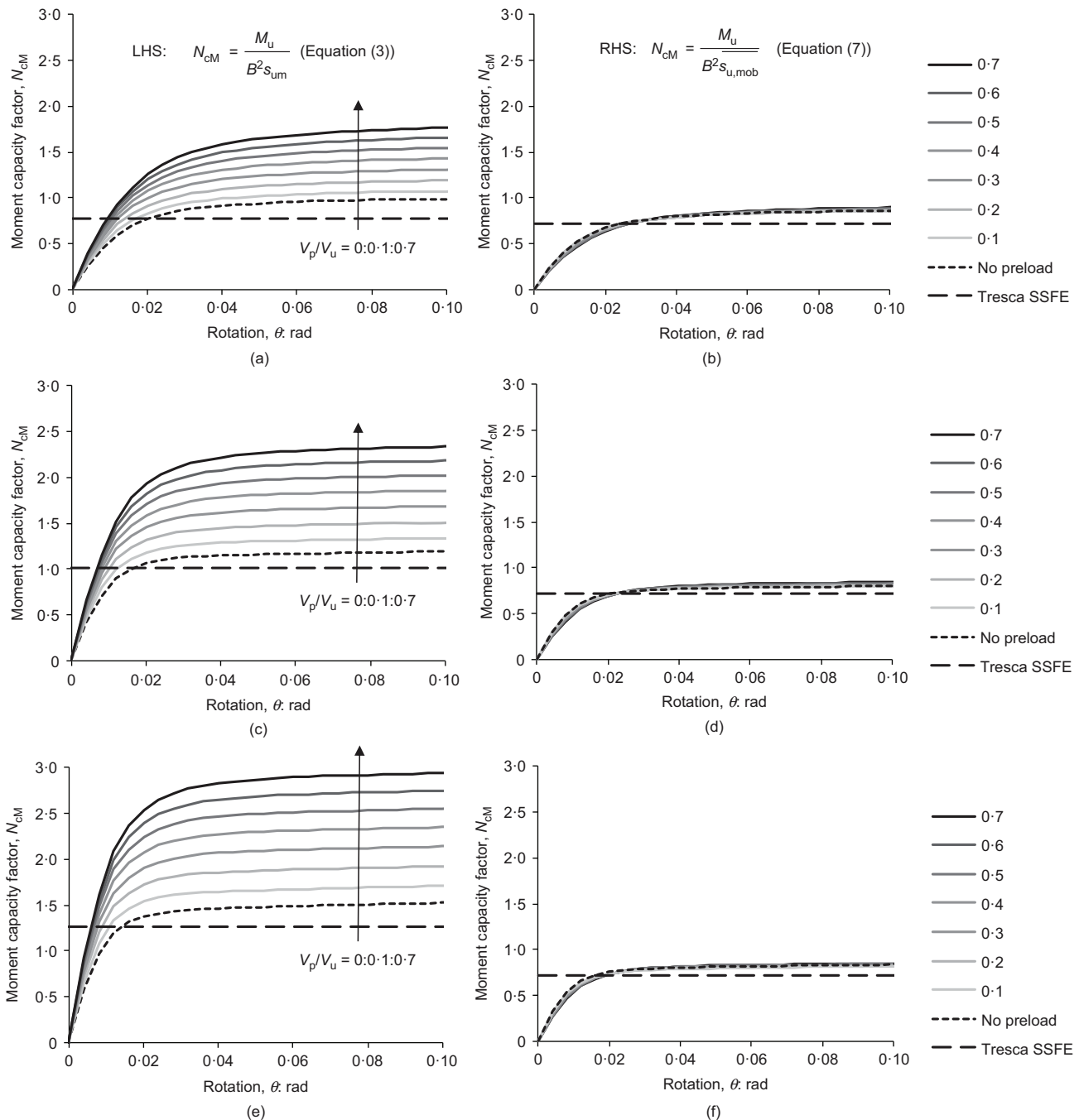


Fig. 4. Moment bearing capacity (conventional normalisation, alternative normalisation): (a), (b) $kBl/s_{um} = 0.4$; (c), (d) $kBl/s_{um} = 2.0$; and (e), (f) $kBl/s_{um} = 4.0$

even when the failure mechanism visibly changes shape as a result of the preload period and localised changes in soil strength due to consolidation. This is best illustrated in Fig. 5, which presents the instantaneous velocity fields at failure for all of the vertical bearing capacity analyses. The mechanisms vary both with strength profile and applied preload. However, the bearing capacity factor N_{cv} is approximately constant when calculated using the mobilised strength $\bar{s}_{u,mob}$ as in equation (5), rather than the mudline strength s_{um} as defined in equation (1). In other words, the change in form of the mechanism has an insignificant influence on the bearing capacity factor as defined herein using the average mobilised undrained strength, $\bar{s}_{u,mob}$, rather than using an in situ strength at a particular depth (typically the mudline).

This observation is important. It means that the proportional increase in $\bar{s}_{u,mob}$ is also the factor by which the bearing capacity increases for a given level of consolidation: changes in $\bar{s}_{u,mob}$ give proportional changes in bearing capacity. Therefore, if this change in strength can be predicted in a simple way for a given initial strength profile, foundation shape and preload period, it can then be applied to the unconsolidated capacity calculated using standard bearing capacity factors relevant to the initial strength profile. This observation also has parallels with prediction of the pre-failure load-deformation response: changes in the soil stress-strain curve can be scaled into similar changes in load-displacement response, without considering any change in the deformation mechanism (Osman & Bolton, 2005; McMahon *et al.*, 2013; Madabhushi & Haigh, 2015).

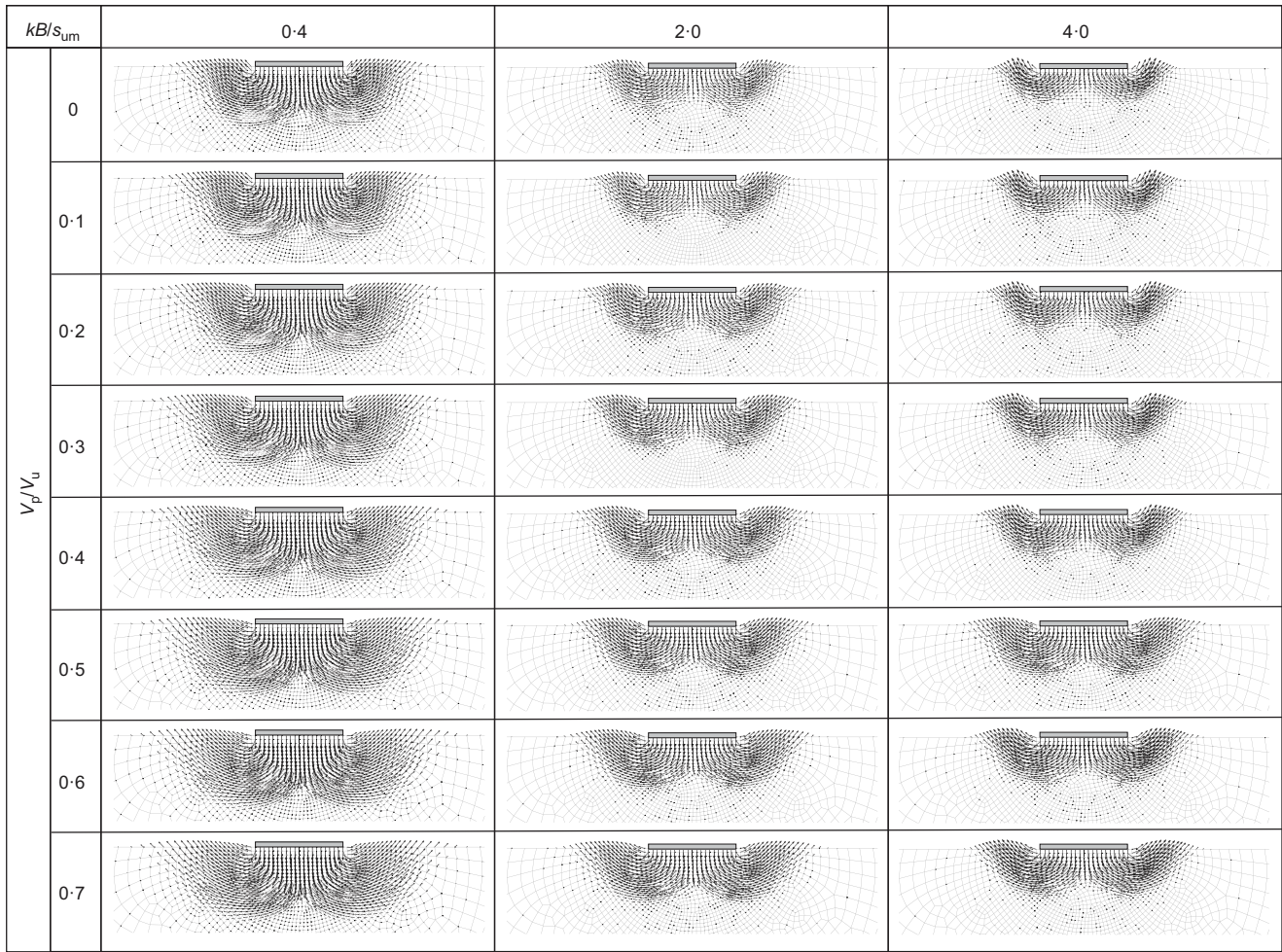


Fig. 5. Instantaneous velocity fields at failure for vertical bearing mechanisms, which all result in approximately constant N_{cv} when calculated using the mobilised strength $\bar{s}_{u,mob}$ as in equation (5), rather than the mudline strength s_{um} as in equation (1)

Ratios of consolidated to unconsolidated average mobilised undrained strength ($\bar{s}_{u,mob,cons}/\bar{s}_{u,mob}$) and subsequently the consolidated to unconsolidated bearing capacity factors ($N_{cv,cons}/N_{cv}$; $N_{ch,cons}/N_{ch}$; $N_{cm,cons}/N_{cm}$) were derived for each strength profile modelled and are presented in Fig. 6. For all loading types the change in average mobilised undrained strength, $\bar{s}_{u,mob}$, accounts almost completely for the change in foundation capacity as the bearing capacity factors back-calculated are all within $\pm 2\%$ of the value obtained for the analysis with no maintained preload period.

Simple prediction model

There is a linear relationship between preload, V_p/B , and gain in $\bar{s}_{u,mob}$, which is amenable to modelling using the following relationship proposed by Gourvenec *et al.* (2014) and Feng & Gourvenec (2015)

$$\Delta \bar{s}_{u,mob} = f_\alpha f_{s_u} R \left(\frac{V_p}{B} \right) \quad (17)$$

where R is the normally consolidated undrained strength ratio of the soil (i.e. s_u/σ'_{v0} ; 0.29 in this instance) and $f_\alpha f_{s_u}$ is a scaling parameter accounting for the non-uniform distributions of stress and strength gain beneath the foundation as a result of the preloading (in overconsolidated conditions, the scaling is separated into two components, hence the pair of f parameters). This approach can

then be used to determine the ratio of consolidated to unconsolidated capacity for different preload ratios, as follows

$$\frac{V_{u,cons}}{V_u}, \frac{H_{u,cons}}{H_u}, \frac{M_{u,cons}}{M_u} = 1 + \frac{\Delta \bar{s}_{u,mob}}{\bar{s}_{u,mob}(V_p/V_u=0)} \quad (18)$$

A best fit to the strength gain modelled in the vertical loading analyses was achieved using a constant value of $f_\alpha f_{s_u}$ of 0.4, which is close to the value of 0.36 ($f_\alpha=0.8$ and $f_{s_u}=0.45$: $f_\alpha f_{s_u}=0.36$) found by Gourvenec *et al.* (2014) for a plane-strain surface foundation and slightly less than the value of 0.45 found by Chatterjee *et al.* (2014) for a plane-strain pipeline.

Similarly, best fits were achieved for the horizontal loading analyses using a constant value of $f_\alpha f_{s_u}$ of 0.7. This is less than the value of 0.919 found by Feng and Gourvenec (2015) for a rectangular mudmat with length-to-width ratio (L/B) equal to 2 on normally consolidated soil. This reflects that the stress and strength gain distributions beneath a plane-strain foundation differ from those that occur beneath a three-dimensional foundation.

Conversely for the moment loading analyses, best fits were achieved with values of 0.55, 0.46 and 0.4 for the soil profiles with kB/s_{um} of 0.4, 2 and 4, respectively. This trend is in general agreement with Feng & Gourvenec's (2015) three-dimensional simulations of a rectangular mudmat foundation (with $L/B=2$) for kB/s_{um} of 1.86 and 3.72 (dependent on the orientation of loading). Their best fits across the same

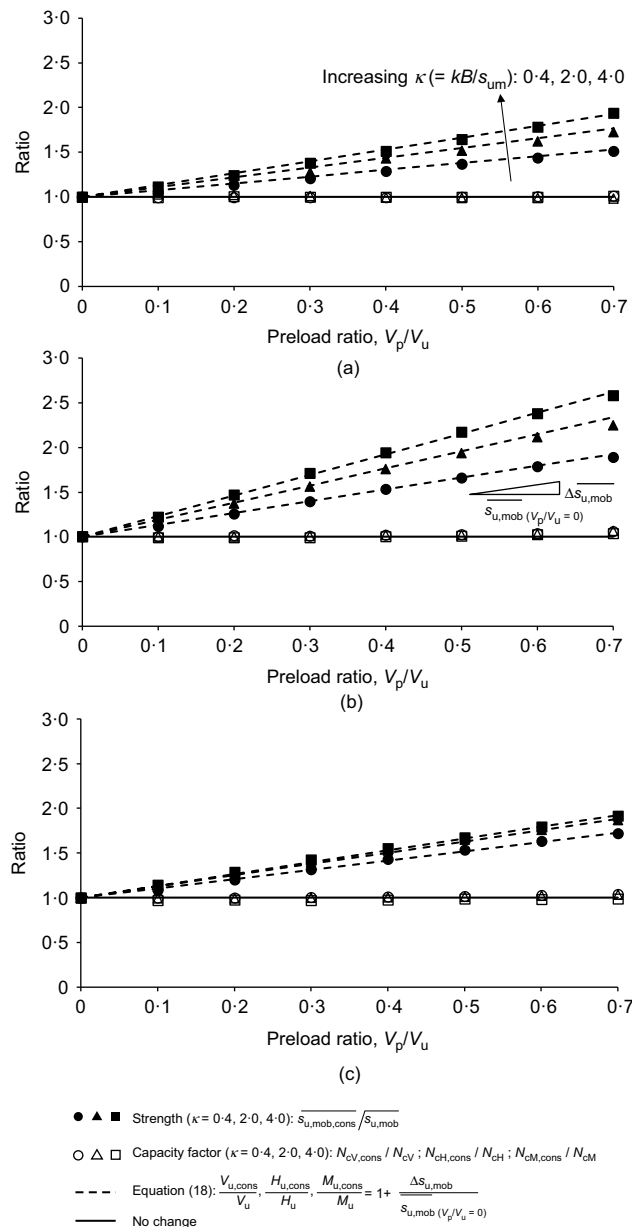


Fig. 6. Comparison of relative importance of strength and mechanism changes for: (a) vertical bearing capacity; (b) horizontal bearing capacity; and (c) moment bearing capacity

range of preload ratio were $f_{\alpha f_{s_u}}$ of 0.538 and 0.345, respectively.

The performance of equation (18) in predicting the vertical, horizontal and moment capacities for preload ratios, V_p/V_u , in the range of 0.1–0.7 (adopting the $f_{\alpha f_{s_u}}$ values outlined in the previous paragraphs) is illustrated in Fig. 7. The differences between the model predictions and the capacities yielded in the finite-element simulations are generally less than 5%.

It appears that appropriate values of $f_{\alpha f_{s_u}}$ for this simple model vary slightly with geometry (i.e. plane-strain foundation, rectangular foundation or plane-strain pipeline) and in the case of moment loading are dependent on the initial soil profile (kB/s_{um}). However, in all cases the changes in soil strength control the increase in capacity for vertical, horizontal and moment loading, and not any change in failure mechanism. This gain is readily predictable using equations (17) and (18) when the bearing capacity factor is defined using equations (5)–(7).

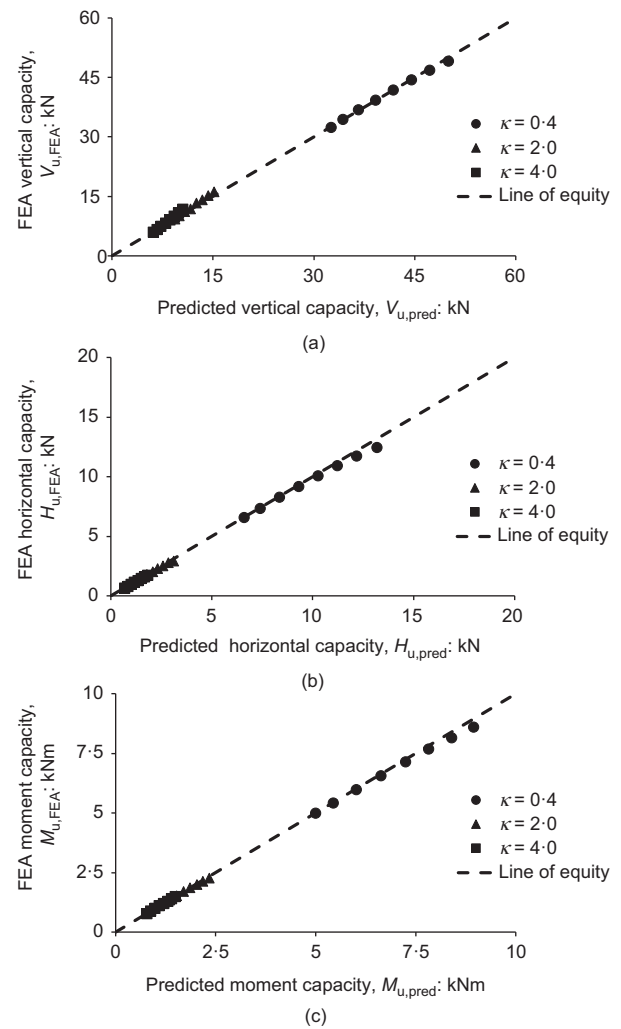


Fig. 7. Comparison of simulated and predicted capacity for preloads, V_p/V_u , in the range of 0–0.7 and $\kappa (= kB/s_{um})$ of 0.4, 2.0 and 4.0: (a) vertical loading; (b) horizontal loading; and (c) moment loading (FEA, finite-element analysis)

CONCLUSIONS

This study has separated the effects of strength gain and changes in mechanism on bearing capacity by defining an operative strength explicitly as the average strength mobilised in the failure mechanism. This allows N_c to be defined as a purely geometric quantity, which allows any change in bearing capacity associated with a change in failure mechanism to be identified.

The results indicate that although the failure mechanism may change – by way of the shear zones and slip planes migrating to preferential locations – this leads to minimal changes in N_{cv} , N_{ch} or N_{cm} . Instead, the gain in capacity is almost entirely due to changes in s_u mobilised within the mechanism. This observation should encourage future studies into consolidated bearing capacity to present gains in capacity in terms of changes in mobilised strength rather than changes in bearing capacity factors.

ACKNOWLEDGEMENTS

This work forms part of the activities of the Centre for Offshore Foundation Systems (COFS), supported as a node of the Australian Research Council's Centre of Excellence for Geotechnical Science and Engineering (CE110001009), and the Industrial Transformation Research Hub in Offshore

Floating Facilities, supported by Shell, Woodside, Lloyds Register and Bureau Veritas (ARC grant IH140100012). The first author is supported by ARC DECRA Fellowship DE170100119. The second author is supported by the Shell EMI Chair in Offshore Engineering at the University of Western Australia. This support is gratefully acknowledged.

NOTATION

| | |
|-------------------------------|---|
| a | critical state model parameter |
| B | foundation width |
| e_{cons} | consolidated voids ratio |
| e_{cs} | void ratio on critical state line at $p'=1$ kPa |
| e_N | void ratio on normal consolidation line at $p'=1$ kPa |
| e_0 | initial void ratio |
| f_{su} | scaling parameter for non-uniform distribution of strength gain |
| f_σ | scaling parameter for non-uniform distribution of stress |
| H_u | ultimate horizontal capacity |
| K_0 | earth pressure coefficient at rest |
| k | gradient of strength with depth |
| M | critical state strength parameter |
| M_u | ultimate moment capacity |
| N_{cH} | bearing capacity factor for horizontal loading |
| N_{cM} | bearing capacity factor for moment loading |
| N_{cv} | bearing capacity factor for vertical loading |
| p'_c | mean effective stress during consolidation |
| p'_0 | initial mean effective stress |
| q_0 | initial deviatoric stress |
| s_u | undrained shear strength |
| $s_{\text{u,cons}}$ | consolidated undrained shear strength |
| s_{um} | undrained shear strength at mudline |
| $\overline{s}_{\text{u,mob}}$ | mobilised undrained strength |
| $s_{\text{u,mob,cons}}$ | consolidated mobilised undrained strength |
| V | volume |
| V_p | vertical preload |
| V_u | ultimate vertical load |
| γ'_c | effective unit weight |
| $\Delta\gamma$ | incremental shear strain |
| ε_v | volumetric strain |
| κ | slope of swelling line |
| Λ | plastic compression ratio |
| λ | slope of normal consolidation line |
| v | Poisson ratio |
| σ'_{v0} | effective vertical stress |
| ϕ_{tc} | friction angle for triaxial compression |

REFERENCES

- Bienen, B. & Cassidy, M. J. (2013). Setup and resulting punch-through risk of jack-up spudcans during installation. *J. Geotech. Geoenvir. Engng* **139**, No. 12, 2048–2059.
- Bransby, M. F. (2002). The undrained inclined load capacity of shallow foundations after consolidation under vertical loads. In *Numerical models in geomechanics: proceedings of the 8th international symposium (NUMOG VIII)* (eds G. N. Pande and S. Pietruszczak), pp. 431–437. Rotterdam, the Netherlands: Balkema.
- Chatterjee, S., Gourvenec, S. & White, D. J. (2014). Assessment of the consolidated breakout response of partially embedded seabed pipelines. *Géotechnique* **64**, No. 5, 391–399, <https://doi.org/10.1680/geot.13.P.215>.
- Feng, X. & Gourvenec, S. M. (2015). Consolidated undrained load-carrying capacity of subsea mudmats under combined loading in six degrees of freedom. *Géotechnique* **65**, No. 7, 563–575, <https://doi.org/10.1680/geot.14.P.090>.
- Feng, X. & Gourvenec, S. (2016). Modelling sliding resistance of tolerably mobile subsea mudmats. *Géotechnique* **66**, No. 6, 490–499, <https://doi.org/10.1680/jgeot.15.P.178>.
- Fu, D., Gaudin, C., Tian, Y., Bienen, B. & Cassidy, M. J. (2015). Effects of preloading with consolidation on undrained bearing capacity of skirted circular footings. *Géotechnique* **65**, No. 3, 231–246, <https://doi.org/10.1680/geot.14.P.2120>.
- Gaone, F. M., Gourvenec, S. & Doherty, J. P. (2018). Large-scale shallow foundation load tests on soft clay – at the National Field Testing Facility (NFTF), Ballina, NSW, Australia. *Special Issue of Comput. Geotech.* **93**, 253–268, <https://doi.org/10.1016/j.compgeo.2017.05.008>.
- Gourvenec, S. M. & Randolph, M. F. (2003). Effect of strength non-homogeneity on the shape of failure envelopes for combined loading of strip and circular foundations on clay. *Géotechnique* **53**, No. 6, 575–586, <https://doi.org/10.1680/geot.2003.53.6.575>.
- Gourvenec, S. M., Vulpe, C. & Murthy, T. G. (2014). A method for predicting the consolidated undrained bearing capacity of shallow foundations. *Géotechnique* **64**, No. 3, 215–225, <https://doi.org/10.1680/geot.13.P.101>.
- Lehane, B. M. & Gaudin, C. (2005). Effects of drained pre-loading on the performance of shallow foundations on over-consolidated clay. In *ASME 2005 24th international conference on offshore mechanics and arctic engineering (OMAE 2005)*, vol. 2, pp. 891–896, paper OMAE2005-67559. New York, NY, USA: American Society of Mechanical Engineers.
- Lehane, B. M. & Jardine, R. J. (2003). Effects of long-term preloading on the performance of a footing on clay. *Géotechnique* **53**, No. 8, 689–695, <https://doi.org/10.1680/geot.2003.53.8.689>.
- Madabhushi, S. S. C. & Haigh, S. K. (2015). Investigating the changing deformation mechanism beneath shallow foundations. *Géotechnique* **65**, No. 8, 684–693, <https://doi.org/10.1680/geot.14.P.226>.
- Mahmoodzadeh, H., Wang, D. & Randolph, M. F. (2015). Interpretation of piezoball dissipation testing in clay. *Géotechnique* **65**, No. 10, 831–842, <https://doi.org/10.1680/geot.14.P.213>.
- McMahon, B., Haigh, S. K. & Bolton, M. D. (2013). Optimal displacement mechanisms beneath shallow foundations on linear-elastic perfectly plastic soil. *Géotechnique* **63**, No. 16, 1447–1450, <https://doi.org/10.1680/geot.13.T.002>.
- Osman, A. S. & Bolton, M. D. (2005). Simple plasticity-based prediction of the undrained settlement of shallow circular foundations on clay. *Géotechnique* **55**, No. 6, 435–447, <https://doi.org/10.1680/geot.2005.55.6.435>.
- Stanier, S. A., Ragni, R., Bienen, B. & Cassidy, M. J. (2014). Observing the effect of sustained loading on spudcans in clay. *Géotechnique* **64**, No. 11, 918–926, <https://doi.org/10.1680/geot.14.P003>.
- Stewart, D. P. (1992). *Lateral loading of piled bridge abutments due to embankment construction*. PhD thesis, The University of Western Australia, Crawley, Australia.
- Vulpe, C. & White, D. J. (2014). Effect of prior loading cycles on vertical bearing capacity of clay. *Int. J. Phys. Modelling Geotech.* **14**, No. 4, 88–98.
- Vulpe, C., Gourvenec, S. & Cornelius, A. (2016a). Effect of embedment on consolidated undrained capacity of skirted circular foundations in soft clay under planar loading. *Can. Geotech. J.* **54**, No. 2, 158–172, <https://doi.org/10.1139/cjg-2016-0265>.
- Vulpe, C., Gourvenec, S., Leman, B. & Fung, K. N. (2016b). Failure envelopes for consolidated undrained capacity of strip and circular surface foundations. *ASCE J. Geotech. Geoenvir. Engng* **142**, No. 8, 04016036, [https://doi.org/10.1061/\(ASCE\)GT.1943-5606.0001498](https://doi.org/10.1061/(ASCE)GT.1943-5606.0001498).
- Wroth, C. P. (1984). The interpretation of in situ soil tests. *Géotechnique* **34**, No. 4, 449–489, <https://doi.org/10.1680/geot.1984.34.4.449>.
- Zdravkovic, L., Potts, D. M. & Jackson, C. (2003). Numerical study of the effect of preloading on undrained bearing capacity. *Int. J. Geomech., ASCE* **3**, No. 1, 1–10.